Progress In Electromagnetics Research C, Vol. 56, 153–162, 2015

An Improved Design of Dual-Band 3 dB 180° Directional Coupler

Bayaner Arigong[1, 4, *], Jin Shao[1, 4], Mi Zhou[1, 4], Han Ren[1, 4], Jun Ding[1], Qianli Mu[2], Yang Li[3], Song Fu[4], Hyoungsoo Kim[1], and Hualiang Zhang[1]

Abstract—A novel design concept of dual-band 180° hybrid ring coupler is presented in this paper. Coupler is a key element in front-end building blocks of wireless transceiver systems such as industrial systems and consumer electronic devices. The proposed design is realized by combining multiple arbitrary length transmission lines operating at two frequencies with one dual-band 180° phase shifter. The even-odd mode method is applied to derive the design equations for proposed dual-band 3 dB 180° directional coupler. Based on the analysis, it is found that the realizable frequency ratio of the proposed coupler is very flexible (i.e., the ratio between the two operating frequencies). Moreover, the 180° phase shifter features arbitrary characteristic impedance (i.e., its characteristic impedance can be arbitrarily chosen), which further ensures the easy implementation of proposed structures. To prove the design concept, full-wave electromagnetic simulations are performed to design a dual-band ring hybrid coupler working at 0.9 and 1.98 GHz. An experimental prototype is fabricated on Rogers RT/Duroid 5880 board. The measurement results match well with the theoretical and numerical ones.

1. INTRODUCTION

The dual-band/multiband and wideband transceiver architectures [1–3] have attracted great interest in electronic industries in recent years since they can simultaneously support multiple frequency bands for consumers to meet their requirement of multi-task and multi-function operations in modern wireless communication systems. The passive microwave circuits such as transmission lines [4, 5], phase shifters [6], filters [7–9], duplexers [10], power dividers [11–15], baluns [16, 17] and directional couplers [18, 19] are key components for radio frequency (RF) transceiver systems. Specifically, the hybrid couplers are fundamental and important components [20–22], which are widely used in microwave, millimeter-wave, and even terahertz circuits. For example, in RF front-end circuits, the hybrid couplers are indispensable components for mixers, balanced mixers, balanced power amplifiers, low noise amplifiers, and beam forming phase array circuits. Among all the hybrid couplers, the conventional 180° coupler (or rat-race coupler) [4] is constructed by transmission lines with entire ring circumference of 1.5λ at its operating frequency, which is too big for practical applications such as in the CMOS technology. In the past, several works [23–25] have been published to design compact 3 dB 180° directional couplers. One of the approaches is focusing on using folded lines or loaded lines to reduce the physical area, and another method is applying lumped components such as capacitors and inductors to miniaturize the coupler size. However, all of these methods suffer from performance degradation of the circuits, and they are operating at single frequency. Therefore, it is difficult to design dual-band 180° couplers based on them. To address this issue, several papers [26, 27] presented dual-band 180° coupler designs. One of the methods is applying shunted stubs on each section of the coupler to realize dual-band operation.

Received 12 January 2015, Accepted 16 March 2015, Scheduled 19 March 2015

* Corresponding author: Bayaner Arigong (BayanerArigong@my.unt.edu).

[1] Department of Electrical Engineering, University of North Texas, Denton, TX 76207, USA. [2] Infineon Technologies, San Jose, CA 95037, USA. [3] Department of Electrical and Computer Engineering, Baylor University, Waco, TX 76798, USA. [4] Department of Computer Science and Engineering, University of North Texas, Denton, TX 76207, USA.

Another solution is adding single shunted stub to the center of the longest branch line (among the four branches of the coupler) for dual-band applications. However, the frequency ratio (i.e., ratio between the two working frequencies) of these coupler designs is still limited to a small range. Also the design theory of them is complex.

In this paper, a novel design of dual-band rat-race coupler which is composed of simple transmission lines and phase shifters has been considered. The proposed design has the following characteristics: 1) the same transmission line is applied to all four branches of the coupler to support dual-band operations (more details will be discussed in Section 2.2); 2) only one dual-band line with multiple transmission line sections (i.e., a dual-band 180° phase shifter) is applied in the proposed dual-band 180° coupler; 3) the characteristic impedance of the transmission line-based dual-band 180° phase shifter can be arbitrary. All these features have led to the dual-band rat-race coupler with flexible frequency ratios due to the flexibility in choosing the electrical lengths of transmission lines.

The whole paper is organized as follows. In Section 2, the basic analysis method and equations are presented to explain the design procedure of proposed dual-band rat-race coupler. In Section 3, to verify the proposed design concept, numerical simulations are conducted to design a dual-band coupler with a frequency ratio of 2.2. The experiment is performed on the dual-band rat-race coupler with four identical branch lines and one 180° phase shifter to validate the design theory. The conclusion is presented in the last section.

2. THEORETICAL ANALYSIS

The topology of proposed dual-band 3 dB 180° directional coupler is shown in Fig. 1. In this general schematic, four identical transmission line sections and a 180° phase shifter are applied. Here, Y denotes the characteristic admittance of each branch, and Θ represents the electrical length of each section as labeled in Fig. 1. Half-wavelength transmission line with arbitrary characteristic impedance is employed to realize the 180° phase shifter. To explain the working principle of this coupler, we will first derive design equations for a generalized single-band 3 dB 180° hybrid coupler (as shown in Fig. 2). Based on this design, the design theory of the proposed dual-band 180° coupler is presented.

Figure 1. The structure of proposed dual-band 3 dB 180° directional coupler.

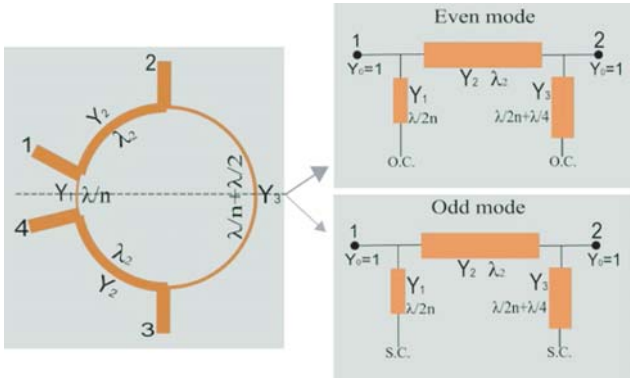

Figure 2. General structure of the single-band 3 dB 180° directional coupler with arbitrary branch lengths.

2.1. Theoretical Analysis of a Generalized Single-Band 180° Hybrid Ring Coupler

The structure of the single-band generalized 180° hybrid coupler is shown in the left of Fig. 2, where the length and impedance of each branch have been marked. Based on the even-odd mode analysis, this 4-port network is decomposed into two 2-port networks as shown in the right of Fig. 2. Here we assume $a = \tan(\beta l_1/2)$, $b = \tan(\beta l_3/2)$, $C = \cos\beta l_2$, and $D = \sin\beta l_2$, where $l_1 = \lambda/n$, $l_2 = \lambda_2$, and

$l_3 = \lambda/n + \lambda/2$. The $ABCD$ matrix under the even-mode excitation is:

$$\begin{aligned}\begin{bmatrix} A & B \\ C & D \end{bmatrix}_e &= \begin{bmatrix} 1 & 0 \\ jY_1a & 1 \end{bmatrix}\begin{bmatrix} C & \frac{j}{Y_2}D \\ jY_2D & C \end{bmatrix}\begin{bmatrix} 1 & 0 \\ jY_3b & 1 \end{bmatrix} \\ &= \begin{bmatrix} C - \frac{Y_3}{Y_2}bD & \frac{j}{Y_2}D \\ j\left[Y_1aC - \frac{Y_1Y_3}{Y_2}abD + (Y_2D + Y_3bC)\right] & C - \frac{Y_1}{Y_2}aD \end{bmatrix}\end{aligned} \tag{1}$$

Under the odd-mode excitation, the $ABCD$ matrix is:

$$\begin{aligned}\begin{bmatrix} A & B \\ C & D \end{bmatrix}_o &= \begin{bmatrix} 1 & 0 \\ -j\frac{Y_1}{a} & 1 \end{bmatrix}\begin{bmatrix} C & \frac{j}{Y_2}D \\ jY_2D & C \end{bmatrix}\begin{bmatrix} 1 & 0 \\ -j\frac{Y_3}{b} & 1 \end{bmatrix} \\ &= \begin{bmatrix} C + \frac{DY_3}{bY_2} & \frac{j}{Y_2}D \\ -j\left[\frac{Y_1C}{a} + \frac{Y_1Y_3}{Y_2}\frac{D}{ab} - \left(Y_2D + Y_3\frac{C}{b}\right)\right] & C + \frac{Y_1}{Y_2}\frac{D}{a} \end{bmatrix}\end{aligned} \tag{2}$$

$$\begin{aligned}
S_{11}^e =& \frac{A + \frac{B}{Z_0} - CZ_0 - D}{A + \frac{B}{Z_0} + CZ_0 + D} \\
=& \frac{aDY_0Y_1 - bDY_0Y_3 - j\left[aCY_1Y_2 - abDY_1Y_3 - DY_0^2 + DY_2^2 + bCY_2Y_3\right]}{2CY_0Y_2 - (bDY_0Y_3 + aDY_0Y_1) + j\left[aCY_1Y_2 - abDY_1Y_3 - DY_0^2 + DY_2^2 + bCY_2Y_3\right]} \\
S_{21}^e =& \frac{2(AD - BC)}{A + \frac{B}{Z_0} + CZ_0 + D} \\
=& \frac{2Y_0Y_2}{2CY_0Y_2 - (bDY_0Y_3 + aDY_0Y_1) + j\left[aCY_1Y_2 - abDY_1Y_3 + DY_0^2 + DY_2^2 + bCY_2Y_3\right]} \\
S_{11}^o =& \frac{A + \frac{B}{Z_0} - CZ_0 - D}{A + \frac{B}{Z_0} + CZ_0 + D} \\
=& \frac{-\frac{D}{a}Y_0Y_1 + \frac{D}{b}Y_0Y_3 + j\left[\frac{C}{a}Y_1Y_2 + \frac{D}{ab}Y_1Y_3 + DY_0^2 - DY_2^2 + \frac{C}{b}Y_2Y_3\right]}{2CY_0Y_2 + \left(\frac{D}{b}Y_0Y_3 + \frac{D}{a}Y_0Y_1\right) - j\left[\frac{C}{a}Y_1Y_2 + \frac{D}{ab}Y_1Y_3 - DY_0^2 - DY_2^2 + \frac{C}{b}Y_2Y_3\right]} \\
S_{21}^o =& \frac{2(AD - BC)}{A + \frac{B}{Z_0} + CZ_0 + D} \\
=& \frac{2Y_0Y_2}{2CY_0Y_2 + \left(\frac{D}{b}Y_0Y_3 + \frac{D}{a}Y_0Y_1\right) - j\left[\frac{C}{a}Y_1Y_2 + \frac{D}{ab}Y_1Y_3 - DY_0^2 - DY_2^2 + \frac{C}{b}Y_2Y_3\right]} \\
S_{11} =& \frac{1}{2}\left\{\frac{aDY_0Y_1 - bDY_0Y_3 - j\left[aCY_1Y_2 - abDY_1Y_3 - DY_0^2 + DY_2^2 + bCY_2Y_3\right]}{2CY_0Y_2 - (bDY_0Y_3 + aDY_0Y_1) + j\left[aCY_1Y_2 - abDY_1Y_3 + DY_0^2 + DY_2^2 + bCY_2Y_3\right]}\right. \\
&\left. + \frac{-\frac{D}{a}Y_0Y_1 + \frac{D}{b}Y_0Y_3 + j\left[\frac{C}{a}Y_1Y_2 + \frac{D}{ab}Y_1Y_3 + DY_0^2 - DY_2^2 + \frac{C}{b}Y_2Y_3\right]}{2CY_0Y_2 + \left(\frac{D}{b}Y_0Y_3 + \frac{D}{a}Y_0Y_1\right) - j\left[\frac{C}{a}Y_1Y_2 + \frac{D}{ab}Y_1Y_3 - DY_0^2 - DY_2^2 + \frac{C}{b}Y_2Y_3\right]}\right\} \\
S_{21} =& \frac{1}{2}\left\{\frac{2Y_0Y_2}{2CY_0Y_2 - (bDY_0Y_3 + aDY_0Y_1) + j\left[aCY_1Y_2 - abDY_1Y_3 + DY_0^2 + DY_2^2 + bCY_2Y_3\right]}\right. \\
&\left. + \frac{2Y_0Y_2}{2CY_0Y_2 + \left(\frac{D}{b}Y_0Y_3 + \frac{D}{a}Y_0Y_1\right) - j\left[\frac{C}{a}Y_1Y_2 + \frac{D}{ab}Y_1Y_3 - DY_0^2 - DY_2^2 + \frac{C}{b}Y_2Y_3\right]}\right\} \\
S_{31} =& \frac{1}{2}\left\{\frac{2Y_0Y_2}{2CY_0Y_2 - (bDY_0Y_3 + aDY_0Y_1) + j\left[aCY_1Y_2 - abDY_1Y_3 + DY_0^2 + DY_2^2 + bCY_2Y_3\right]}\right. \\
&\left. - \frac{2Y_0Y_2}{2CY_0Y_2 + \left(\frac{D}{b}Y_0Y_3 + \frac{D}{a}Y_0Y_1\right) - j\left[\frac{C}{a}Y_1Y_2 + \frac{D}{ab}Y_1Y_3 - DY_0^2 - DY_2^2 + \frac{C}{b}Y_2Y_3\right]}\right\}
\end{aligned} \tag{3}$$

$$S_{41} = \frac{1}{2}\left\{ \frac{aDY_0Y_1 - bDY_0Y_3 - j\left[aCY_1Y_2 - abDY_1Y_3 - DY_0^2 + DY_2^2 + bCY_2Y_3\right]}{2CY_0Y_2 - (bDY_0Y_3 + aDY_0Y_1) + j\left[aCY_1Y_2 - abDY_1Y_3 + DY_0^2 + DY_2^2 + bCY_2Y_3\right]} - \frac{-\frac{D}{a}Y_0Y_1 + \frac{D}{b}Y_0Y_3 + j\left[\frac{C}{a}Y_1Y_2 + \frac{D}{ab}Y_1Y_3 + DY_0^2 - DY_2^2 + \frac{C}{b}Y_2Y_3\right]}{2CY_0Y_2 + \left(\frac{D}{b}Y_0Y_3 + \frac{D}{a}Y_0Y_1\right) - j\left[\frac{C}{a}Y_1Y_2 + \frac{D}{ab}Y_1Y_3 - DY_0^2 - DY_2^2 + \frac{C}{b}Y_2Y_3\right]} \right\}$$

Based on Equations (1), (2), the corresponding S_{11}^e, S_{21}^e, S_{11}^o and S_{21}^o can be calculated and are given in Equation (3). With the S_{11}^e, S_{21}^e, S_{11}^o and S_{21}^o, the four-port network S-parameters can be derived as:

$$S_{11} = \frac{1}{2}\left(S_{11}^e + S_{11}^o\right) \tag{4a}$$

$$S_{21} = \frac{1}{2}\left(S_{21}^e + S_{21}^o\right) \tag{4b}$$

$$S_{31} = \frac{1}{2}\left(S_{21}^e - S_{21}^o\right) \tag{4c}$$

$$S_{41} = \frac{1}{2}\left(S_{11}^e - S_{11}^o\right) \tag{4d}$$

The derived equations for these S-parameters are again given in Equation (3) (at the bottom of it). Since the hybrid coupler is a reciprocal and symmetric 4-port network, the following three conditions need to be satisfied for its proper operation.

1) Two output ports and two input ports are isolated from each other. Thus $S_{31} = S_{42} = 0$.
2) The input port needs to be matched. Thus $S_{11} = 0$.
3) The 3 dB coupler features equal power division at the output port 2 and 4. Thus $|S_{21}| = |S_{41}|$.
4) Based on these conditions, we can generalize design formulas as shown below.

$$-bY_3 - aY_1 = \frac{1}{b}Y_3 + \frac{1}{a}Y_1 \tag{5}$$

$$\left(a + \frac{1}{a}\right)CY_1Y_2 + \left(b + \frac{1}{b}\right)CY_2Y_3 = \left(ab - \frac{1}{ab}\right)DY_1Y_3 \tag{6}$$

$$\left(\frac{1}{a} - a\right)CY_1Y_2 + \left(ab + \frac{1}{ab}\right)DY_1Y_3 + \left(\frac{1}{b} - b\right)CY_2Y_3 + 2DY_0^2 - 2DY_2^2 = 0 \tag{7}$$

$$4Y_2 = \left(a + \frac{1}{a}\right)DY_1 - \left(b + \frac{1}{b}\right)DY_3 \tag{8}$$

From Equation (5), we can demonstrate that $Y_1 = Y_3$ since $ab = -1$ (since there is a 90° phase difference between a and b), which means that the opposite arms l_1 and l_3 have the same characteristic admittance. By substituting this condition into (6), (7) and (8), the following two equations are derived.

$$(a+b)\,CY_1Y_2 = D\left(Y_0^2 - Y_1^2 - Y_2^2\right) \tag{9}$$

$$2Y_2 = (a-b)DY_1 \tag{10}$$

Utilizing the above two equations, the generalized single-band 3 dB 180° directional coupler with arbitrary branch lengths can be designed.

2.2. Analysis of the Proposed Dual-Band 180° Hybrid Coupler

Based on the single-band 180° coupler, a new dual-band 180° coupler is designed. The general structure of the new coupler is shown in Fig. 1. Since it is composed of four identical transmission lines and a 180° phase shifter, the design principle for these components to support dual-band operations is presented as follows. For the four identical transmission lines, the $ABCD$ matrix is:

$$\begin{bmatrix} A & B \\ C & D \end{bmatrix} = \begin{bmatrix} \cos\theta & j\frac{\sin\theta}{Y} \\ jY\sin\theta & \cos\theta \end{bmatrix} \tag{11}$$

(where Θ is the electrical length and Y the characteristic admittance of the transmission line). For the purpose of dual-band operation, the necessary condition is:

$$\theta_{f2} = m\pi \pm \theta_{f1} \tag{12}$$

Here $\Theta f1$ and $\Theta f2$ are electrical lengths of the line at the two working frequencies ($\Theta f1 < \Theta f2$), and $m = 1, 2, 3, \ldots$. For the electrical lengths of these transmission lines, the following relation is always held at two operating frequencies:

$$\frac{\theta_{f1}}{\theta_{f2}} = \frac{f_1}{f_2} \tag{13}$$

By substituting (12) into (13), it can be further derived as:

$$\theta_{f1} = \frac{m\pi}{1 \pm \frac{f_2}{f_1}} = \frac{m\pi}{1 \pm R} \tag{14}$$

where $R = f_2/f_1$ and $m = 1, 2, 3, \ldots$. According to (14), once the frequency ratio R is selected, the electrical length of the transmission line will be determined. For the proposed coupler to operate at two frequency bands simultaneously, we have employed the same length for two branches (the electrical length of Y_2 is equal to that of Y_1, $\lambda_2 = \lambda/n$ as labeled in the left of Fig. 2). In general, Y_1, Y_2, l_1, and l_2 can be numerically analyzed by solving (9) and (10). In principle, there are many possible solutions as listed in Table 1. Specifically, for the proposed dual-band coupler, since l_1 needs to be equal to l_2, the lengths of them are confined within the range from $\lambda/8$ to $\lambda/4$ according to Table 1 (these lengths are evaluated at the lower operating frequency f_1). Also, since $l_1 = l_2$, according to (9) and (10), Y_1 is equal to Y_2. Therefore, in the proposed dual-band coupler, the transmission lines applied in all four branches are identical and their electrical lengths are calculated by (14).

For the dual-band 180° phase shifter used in the proposed 180° coupler, its general structure is shown in Fig. 3. It is realized by cascading two dual-band 90° transmission lines. The $ABCD$ matrix of each dual-band 90° transmission line is given in (15):

$$\begin{bmatrix} A_T & B_T \\ C_T & D_T \end{bmatrix} = \begin{bmatrix} \cos\theta_a & jZ_a \sin\theta_a \\ \frac{j\sin\theta_a}{Z_a} & \cos\theta_a \end{bmatrix} \begin{bmatrix} 1 & 0 \\ \frac{j\tan\theta_b}{Z_b} & 1 \end{bmatrix} \begin{bmatrix} \cos\theta_a & jZ_a \sin\theta_a \\ \frac{j\sin\theta_a}{Z_a} & \cos\theta_a \end{bmatrix} = \begin{bmatrix} 0 & \pm j\frac{1}{Y_p} \\ \pm jY_p & 0 \end{bmatrix} \tag{15}$$

where Z_a, Z_b, Θ_a, and Θ_b represent the characteristic impedances and electrical lengths of the series and shunted stubs as shown in Fig. 3. Y_p is the characteristic admittance of equivalent $\lambda/4$ transmission line (Note: Y_p can be arbitrary values as will be explained in the end of this section).

For the purpose of dual-band operation of the transmission line, the design equations are derived from (15) and the results are given in (16)–(19).

$$Z_a \tan\theta_{af1} = \pm\frac{1}{Y_p} \tag{16}$$

$$\tan\theta_b = \frac{Z_b\left(\cos^2\theta_a - \sin^2\theta_a\right)}{Z_a \sin\theta_a \cos\theta_a} \tag{17}$$

$$\theta_{af1} = \frac{N\pi}{1 \pm \frac{f_2}{f_1}} = \frac{N\pi}{1 \pm R} \tag{18}$$

$$\theta_{bf1} = \frac{M\pi}{1 \pm \frac{f_2}{f_1}} = \frac{M\pi}{1 \pm R} \tag{19}$$

Here Θ_{af1} and Θ_{bf1} are electrical lengths of series and shunted stubs at the first design frequencies (f_1); Y_p can be any value, $N = 1, 2, 3, \ldots$, and $M = 1, 2, 3, \ldots$. By solving Equations (16)–(19), the design parameters of the dual-band phase shifter can be obtained.

Based on the above discussions and design equations (e.g., Equations (9), (10), (14), (16)–(19)), the proposed dual-band 180° 3 dB directional coupler can be designed.

Finally, an important feature of the proposed dual-band coupler, namely the realizable frequency ratio range, is discussed. In practice, this parameter is often limited by the realizable impedance range of the transmission lines (i.e., microstrip line in this paper). In our analysis, we have assumed that

Table 1. Relation between two branches (i.e., Y_1 and Y_2).

l_1	Y_1	l_2	Y_2
$\lambda/12$	$0.4772 \sim 31.665$	$\lambda/6.3421 \sim \lambda/4$	$0.8944 \sim 52.9691$
$\lambda/10$	$0.5067 \sim 36.222$	$\lambda/6.8228 \sim \lambda/4$	$0.8621 \sim 49.0629$
$\lambda/8$	$0.5774 \sim 161.45$	$\lambda/8 \sim \lambda/4$	$0.8165 \sim 161.45$
$\lambda/6$	$0.6547 \sim 57.626$	$\lambda/15.06 \sim \lambda/4$	$0.756 \sim 26.966$
$\lambda/4$	0.7071	$\lambda/4$	0.7071

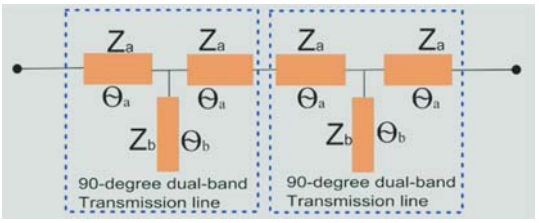

Figure 3. General topology of the 180° dual-band phase shifter used in the proposed coupler.

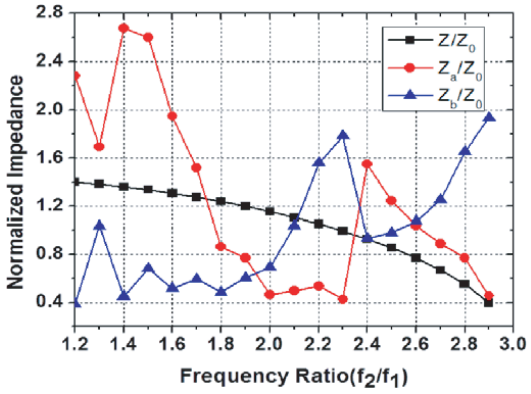

Figure 4. Calculated normalized impedances of different branch lines used in the proposed coupler at different frequency ratios.

the impedance is within the range of 20 to 140 Ω (according to our analysis, these impedances can be realized using the conventional microstrip transmission lines). Following the design procedure, the calculated branch line impedance Z ($Z = 1/Y$ in Fig. 1), and series and shunted impedances of the 180° phase shifter (Z_a and Z_b in Fig. 3) are plotted in Fig. 4 under different frequency ratios (all of these values have been normalized to 50 Ω). It is observed that the frequency ratio from 1.2 to 2.9 can be supported. Moreover, it is worth to point out that the characteristic impedance (i.e., $1/Y_p$ in (21)) of the dual-band 180° phase shifter can be arbitrary. As long as its total phase shift is 180° at the two design frequencies, it will guarantee the performance of the proposed dual-band coupler. This property has ensured that the dual-band 180° phase shifter can support a large range of frequency ratio (since for a specific frequency ratio, we can find a suitable Y_p that is convenient for dual-band operation). For the four identical transmission lines (with an admittance of Y as shown in Fig. 1), its length is within the range of $\lambda/8 - \lambda/4$ (as discussed in Section 2.2). According to Equation (20), it can support the frequency ratio from 1 to 3 when m is 1 in Equation (20). For a frequency ratio beyond that, a different m can be applied to meet the requirement. Overall, the proposed dual-band coupler can support a wide range of frequency ratio with a simple structure.

3. SIMULATION AND MEASUREMENT RESULTS

To verify the design theory of the proposed coupler, a dual-band coupler working at 0.9/1.98 GHz is designed. The electromagnetic simulations results of the designed coupler are shown in Fig. 5. In Fig. 5(a), the simulated insertion losses S_{21}, S_{41}, S_{32} and S_{34} are plotted. It is found that they are around −3 dB at two design frequencies. In Fig. 5(b), the simulated return loss and isolation are shown. As desired, at the two working frequencies, the return loss is better than 45 dB and the isolation is better than 50 dB. The phase responses are shown in Figs. 5(c), (d). As desired, at the two working frequencies, S_{21} and S_{41} are equal-phase, and S_{32} and S_{34} have a 180° phase difference.

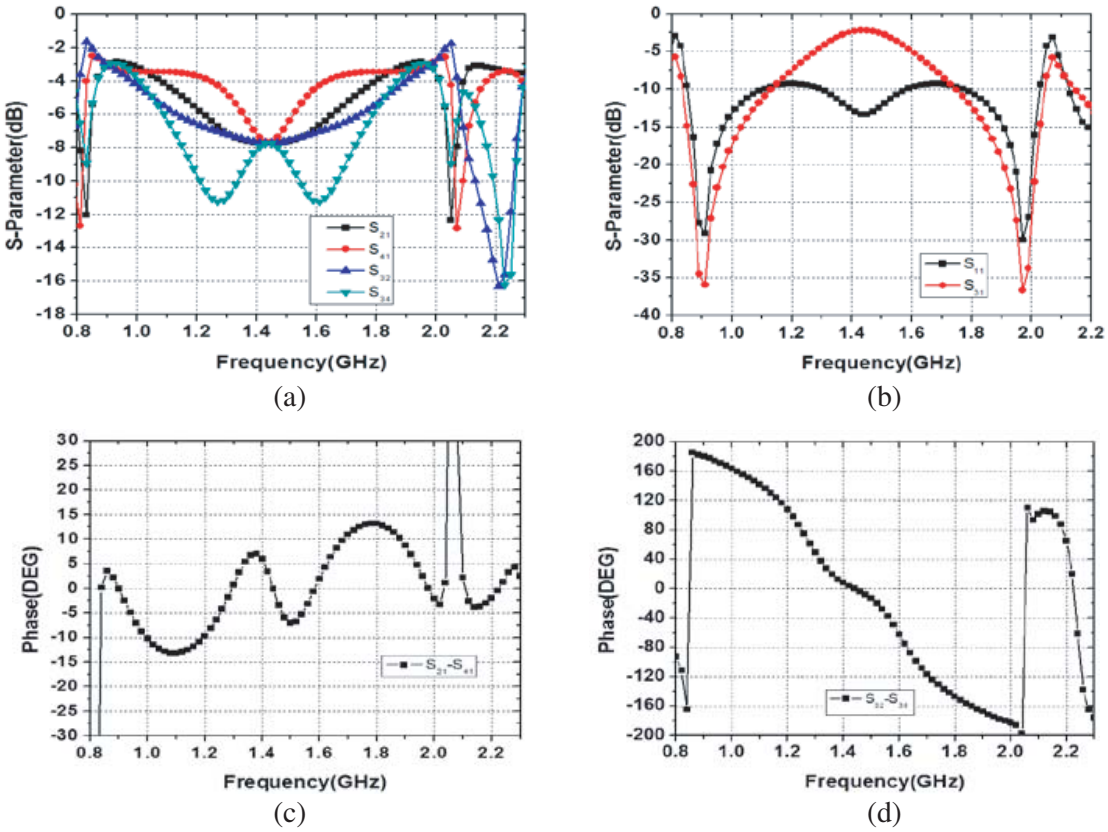

Figure 5. Simulation results of the dual-band 3 dB 180° directional coupler working at 0.9 GHz and 1.98 GHz. (a) Insertion losses. (b) Return loss and isolation. (c) Phase difference between the two output ports (when signal is input from port 1). (d) Phase difference between the two output ports (when signal is input from port 3).

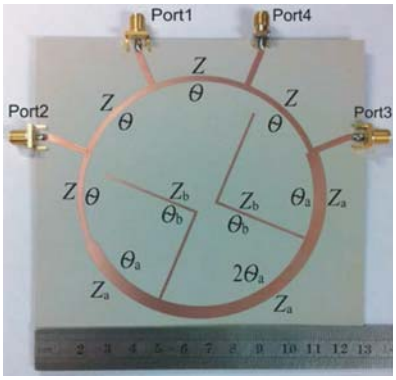

Figure 6. Photo of the fabricated dual-band rat-race coupler.

The designed coupler has been fabricated and characterized experimentally (using Rogers RT/Duroid 5880 board ($\varepsilon_r = 2.2$, $H = 0.787$ mm, and $\tan\delta = 0.0009$)). Fig. 6 shows the photo of the fabricated dual-band 3 dB 180° directional coupler. The design parameters are: $Z = 56.62\,\Omega$, $\theta = 56.25°$, $Z_a = 30.07\,\Omega$, $\theta_a = 56.25°$, $Z_b = 87.63\,\Omega$, $\theta_b = 112.5°$, where the parameters are calculated at the lower design frequency 0.9 GHz. The port impedance is 50 Ω. The measurement results are shown in Fig. 7. A summary of measured performance of this coupler is listed in Table 2. From the experiment results, it is found that the two operating bands are slightly shifted from 0.9/1.98 GHz to 0.94/2.06 GHz

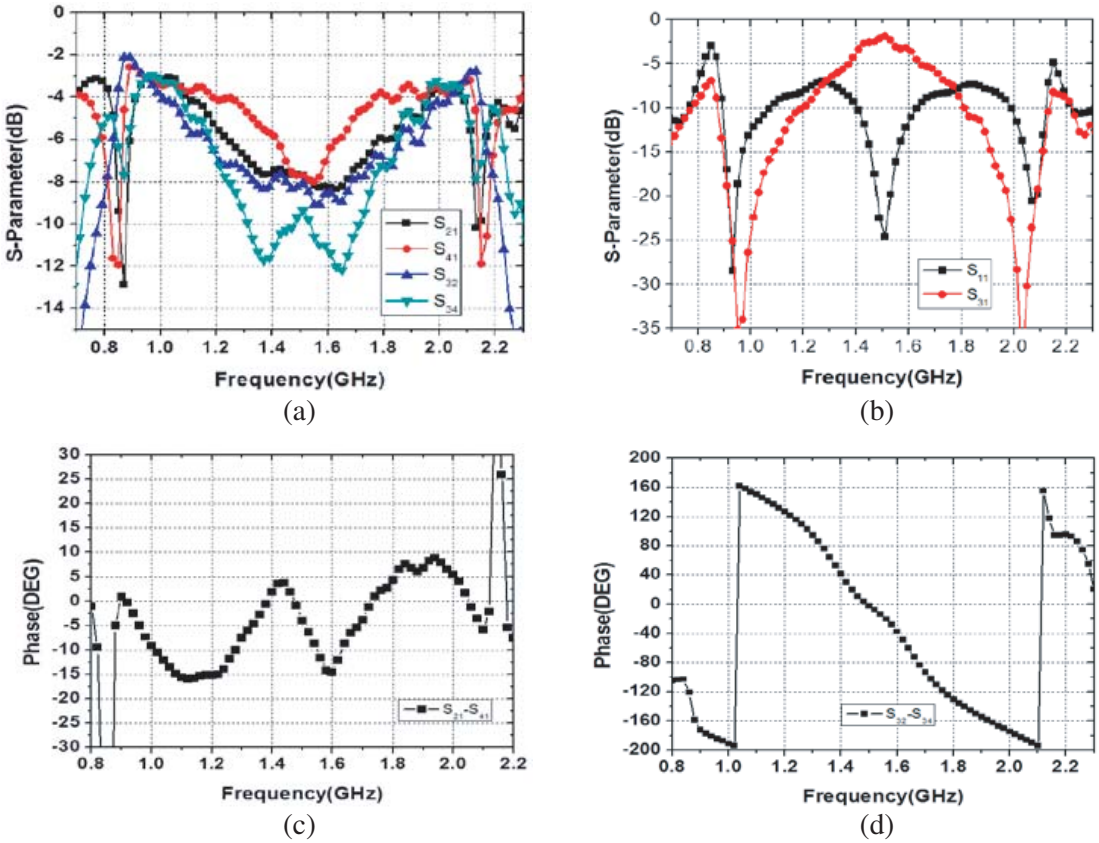

Figure 7. Measurement results of the designed dual-band 3 dB 180° directional coupler. (a) Insertion losses. (b) Return loss and isolation. (c) Phase difference between the two output ports (when signal is input from port 1). (d) Phase difference between the two output ports (when signal is input from port 3).

Table 2. Measured performance of proposed dual-band rat-race coupler.

Frequency	940 MHz	2.06 GHz
Input return loss	22.5 dB	18.6 dB
Isolation	29.2 dB	26.4 dB
Insertion loss (S_{21})	3.2 dB	3.6 dB
Insertion loss (S_{41})	3.0 dB	3.5 dB
$\angle S_{21} - \angle S_{41}$	2.57°	1.3°
Insertion loss (S_{32})	3.0 dB	3.6 dB
Insertion loss (S_{34})	3.2 dB	3.4 dB
$\angle S_{32} - \angle S_{34}$	180.9°	177.1°

which is due to the fabrication errors. From Table 2, the S_{31} (isolation) is less than -26 dB at two design frequencies, and the S_{11} is less than -18 dB at both frequency bands. All the measured insertion losses are around 3 dB at the design frequencies.

Moreover, when the signal is input from port 1, the phase difference between port 2 and port 4 is close to 0° (at most 2.57°). When the signal is input from port 3, the phase difference between port 2 and port 4 is close to 180° (177.1° in the worst case). Considering the amplitude and phase mismatch, the bandwidth of the designed coupler is larger than 50MHz at both two working frequency bands

(Here, the tolerances of amplitude and phase mismatches are 1 dB and 5°, respectively). The amplitude imbalance and phase imbalance are caused by several reasons such as fabrication tolerance, junction loss and variance of substrate parameters. The performance of this work and state-of-the-art dual-band 180° directional couplers is listed in Table 3. In comparison, the proposed design can provide a superior frequency ratio with large design flexibility. Moreover, the dual-band couplers implemented in [26, 27] are based on the conventional rat-race coupler structure. The dual-band coupler presented in this work is implemented based on a generalized rat-race coupler structure, which leads to a more compact size.

Table 3. Performance comparison of this work with the state-of-art dual-band rat-race coupler.

Reference	[26]	[27]	This work
Frequency ratio	$1.75 \sim 2.75$	$1.7 \sim 2.75$	$1.2 \sim 2.9$
ε_r	3.38	6.15	2.2
Bandwidth	50 MHz	140 MHz	50 MHz
Technique	Adding Short shunt stub	Adding open shunt stub	Applying dual-band phase shifter
Size	$0.25\lambda_0 \times 0.5\lambda_0$ λ_0 is the free-space wavelength @1.45 GHz	$0.4\lambda_0 \times 0.78\lambda_0$ λ_0 is the free-space wavelength @1 GHz	$0.35\lambda_0 \times 0.35\lambda_0$ λ_0 is the free-space wavelength @0.9 GHz

4. CONCLUSION

In this paper, a new design of dual-band 3 dB 180° directional coupler is presented. Based on the even-odd mode method, explicit design equations are derived for the proposed design. It is found that a wide range of frequency ratio can be achieved by the proposed dual-band rat-race coupler. Applying the derived design equations, an experimental prototype is designed, simulated, and characterized. Good agreement between the simulation and measurement results has been achieved. It is expected that this new coupler can be readily applied to various dual-band/multiband wireless industrial products.

REFERENCES

1. Chang, S. R., W. Chen, S. Chang, C. Tu, C. Wei, C. Chien, C. Tsai, J. Chen, and A. Chen, "A dual-band RF transceiver for multistandard WLAN applications," *IEEE Trans. Microw. Theory Tech.*, Vol. 55, No. 3, 1048–1055, Mar. 2002.
2. Chen, X.-Q., X.-W. Shi, Y.-C. Guo, and M.-X. Xiao, "A novel dual band transmitter using microstrip defected ground structure," *Progress In Electromagnetics Research*, Vol. 83, 1–11, 2008.
3. Xie, H., X. Wang, L. Lin, H. Tang, Q. Fang, H. Zhao, S. Wang, F. Yao, A. Wang, Y. Zhou, and B. Qin, "A 52-mW 3.1–10.6-GHz fully integrated correlator for IR-UWB transceivers in 0.18 µm CMOS," *IEEE Trans. Ind. Electron.*, Vol. 57, No. 5, 1546–1554, May 2010.
4. Monti, G., R. De Paolis, and L. Tarricone, "Design of a 3-state reconfigurable CRLH transmission line based on MEMS switches," *Progress In Electromagnetics Research*, Vol. 95, 283–297, 2009.
5. Pozar, D. M., *Microwave Engineering*, 4th Edition, Wiley, NJ, 2011.
6. Zheng, S. and W. Chan, "Differential RF phase shifter with harmonic suppression," *IEEE Trans. Ind. Elctron.*, Vol. 61, No. 6, 2891–2899, Jun. 2014.
7. Zhang, H. and K. J. Chen, "A tri-section stepped-impedance resonator for cross-coupled bandpass filters," *IEEE Microw. Wireless Compon. Lett.*, Vol. 15, No. 6, 401–403, Jun. 2005.
8. Fan, J.-W., C.-H. Liang, and D. Li, "Design of cross-coupled dual-band filter with equal-length split-ring resonators," *Progress In Electromagnetics Research*, Vol. 75, 285–293, 2007.

9. Wu, G.-L., W. Mu, D. Li, and Y.-C. Jiao, "Design of novel dual-band bandpass filter with microstrip meander-loop resonator and CSRR DGS," *Progress In Electromagnetics Research*, Vol. 78, 17–24, 2008.
10. Zhou, R., Z. Zhang, C. Chen, and H. Zhang, "Design of dual-band microwave duplexers," *Electron. Lett.*, Vol. 50, No. 3, 219–221, Jan. 2014.
11. Zhang, H. and H. Xin, "Designs of dual-band Wilkinson power dividers with flexible frequency ratios," *IEEE MTT-S. Int. Microwave Symp. Dig.*, Vol. 15, No. 20, 1223–1226, Jun. 2008.
12. Wu, Y., Y. Liu, and S. Li, "An unequal dual-frequency Wilkinson power divider with optional isolation structure," *IEEE Trans. Ind. Electron.*, Vol. 60, No. 10, 4737–4745, Oct. 2013.
13. Wu, Y., Y. Liu, and S. Li, "An unequal dual-frequency Wilkinson power divider with optional isolation structure," *Progress In Electromagnetics Research*, Vol. 91, 393–411, 2009.
14. Lin, Z. and Q.-X. Chu, "A novel approach to the design of dual-band power divider with variable power dividing ratio based on coupled-lines," *Progress In Electromagnetics Research*, Vol. 103, 271–284, 2010.
15. Song, K., Y. Mo, Q. Xue, and Y. Fan, "Wideband four-way out-of-phase slotline power dividers," *IEEE Trans. Ind. Electron.*, Vol. 61, No. 7, 3598–3606, Jul. 2014.
16. Zhang, H., Y. Peng, and H. Xin, "A tapped stepped-impedance balun with dual-band operations," *IEEE Antennas and Wireless Propagation Letters*, Vol. 7, 119–122, 2008.
17. Shao, J., H. Zhang, C. Chen, S. Tan, and K. J. Chen, "A compact dual-band coupled-line balun with tapped open-ended stubs," *Progress In Electromagnetics Research C*, Vol. 22, 109–122, 2011.
18. Nedil, M. and T. A. Denidni, "Analysis and design of an ultra wideband directional coupler," *Progress In Electromagnetics Research B*, Vol. 1, 291–305, 2008.
19. Lopez-Berrocal, B., L. de-Oliva-Rubio, E. Marquez-Segua, A. Moscoso-Martir, I. Molina-Fernandez, and P. Uhlig, "High performance 1.8–18 GHz 10-dB low temperature co-fired ceramic directional coupler," *Progress In Electromagnetics Research*, Vol. 104, 99–112, 2010.
20. Kim, D. and G. Yang, "Design of new hybrid-ring directional coupler using $\lambda/8$ or $\lambda/6$ sections," *IEEE Trans. Microw. Theory Tech.*, Vol. 39, No. 10, 1779–1784, Oct. 1991.
21. Zhang, H. and K. J. Chen, "A stub tapped branch-line coupler for dual-band operations," *IEEE Microw. Wireless Compon. Lett.*, Vol. 17, No. 2, 106–108, Feb. 2007.
22. Wu, Y., S. Y. Zheng, S. Leung, Y. Liu, and Q. Xue, "An analytical design method for a novel dual-band unequal coupler with four arbitrary terminated resistances," *IEEE Trans. Ind. Electron.*, Vol. 61, No. 10, 5509–5516, 2014.
23. Eccleston, K. W. and S. H. M. Ong, "Compact planner microstripline branch-line and rat-race couplers," *IEEE Trans. Microw. Theory Tech.*, Vol. 51, No. 10, 2119–2125, Oct. 2003.
24. Settaluri, R. K., G. Sundberg, A. Weisshaar, and V. K. Tripathi, "Compact folded line rat-race hybrid couplers," *IEEE Trans. Microw. Guided Wave Lett.*, Vol. 10, No. 2, 61–63, Feb. 2000.
25. Hirota, T., A. Minakawa, and M. Muraguchi, "Reduced-size branch-line and rat-race hybrids for uniplanar MMIC's," *IEEE Trans. Microw. Theory Tech.*, Vol. 38, No. 3, 270–275, Mar. 1990.
26. Cheng, K. M. and F. L. Wong, "A novel rat-race coupler design for dual-band applications," *IEEE Microw. Wireless Compon. Lett.*, Vol. 15, No. 8, 521–523, Aug. 2005.
27. Zhang, H. and K. J. Chen, "Design of dual-band rat-race couplers," *IET Microw. Antennas & Propag.*, Vol. 38, No. 3, 270–275, Mar. 2009.